TESLA Report 2003-11

Electro-Optic Sampling at the TESLA Test Accelerator: Experimental Setup and First Results

M. Brunken[a], H. Genz[a], P. Göttlicher[b], C. Hessler[a], M. Hüning[b], H. Loos[a], A. Richter[a], H. Schlarb[b], P. Schmüser[c], S. Simrock[b], D. Suetterlin[d], M. Tonutti[e], D. Türke[e]
[a]Institut für Kernphysik, Technische Universität Darmstadt
[b]Deutsches Elektronen-Synchrotron DESY
[c]Institut für Experimentalphysik, Universität Hamburg
[d]Paul Scherrer Institut, Villigen, Switzerland
[e]Physikalisches Insitut IIIa, RWTH Aachen

Abstract

A mode-locked titanium-sapphire laser with 15 fs pulse width is used to determine the temporal profile of the ultrashort electron bunches in the linear TESLA Test accelerator. The experimental setup is described and first results are presented on the synchronization of the Ti:Sa laser with the radio frequency of the superconducting accelerator and on the coincidence measurements between the laser pulses and the coherent transition radiation pulses generated by the electron bunches. For the next step of the experiment, the electro-optic sensor will be mounted inside the vacuum pipe of the linac to permit a direct measurement of the electric field carried by the relativistic bunches.

1 Introduction

At DESY the first Free Electron Laser (FEL) in the Vacuum Ultraviolet regime has started operation in February 2000. The laser is driven by a 250 MeV superconducting linear electron accelerator. The FEL avoids the conventional optical cavity and is based on the principle of Self Stimulated Spontaneous Emission (SASE) which opens the path to powerful FEL's in the X ray regime where high-reflectivity mirrors for perpendicular incidence do not exist. Electron bunches of high charge density pass through a long undulator magnet and their spontaneous undulator radiation is amplified by the interaction with the relativistic electrons. In order to obtain a high gain or saturation in the FEL, the peak current in the bunches must be very large, in the order of kA. The bunches are longitudinally compressed to achieve the high peak current. This is accomplished by off-crest acceleration in the first module of 8 superconducting cavities followed by a magnetic chicane which provides an energy-dependent path length. In the phase I of the FEL the rms bunch length is about 1 ps in the time domain. For the phase II of the FEL facility, aiming at electron energies of 1 GeV and FEL wavelengths below 10 nm, two bunch compressors will be installed reducing the rms bunch length to 200 fs. Precise measurements of the temporal profile of the compressed electron bunches are essential for the commissioning of the linac and a proper understanding of the bunch compression mechanism including subtle effects such as coherent synchrotron radiation.

Time measurements with a resolution in the 100 fs regime are exceedingly difficult and at the limit of the best streak cameras available. The electro-optic sampling (EOS)

technique [1, 2, 3] has the potential of eventually reaching this resolution. The principle of EOS is as follows: the electric field co-propagating with the relativistic electron bunch induces a birefringence in an optically active crystal like zinc telluride (ZnTe), and this optical anisotropy is sampled by an ultrashort polarized laser pulse. For this purpose, a titanium-sapphire (Ti:Sa) laser is needed with the shortest pulse duration commercially available (below 20 fs). Such a laser has automatically a large bandwidth (65 nm, central wavelength 805 nm). The precise synchronisation of the femtosecond Ti:Sa laser pulses and the picosecond electron bunches in the TTF linac is a challenging task which is tackled in two steps. First, one makes use of the timing structure of the electron linac. The particles are accelerated with superconducting cavities whose resonance frequency is 1.3 GHz. The repetition frequency of the Ti:Sa laser is adjusted to exactly the 16th subharmonic of the RF frequency (81.249975 = 1299.9996/16 MHz). Once this condition is fulfilled the timing of the beam pulses is fixed relative to the laser pulses. However, the electron bunches may be located anywhere between two laser pulses whose spacing is 12.3 ns. To narrow down the time range for the overlap of the two independent signals to about a nanosecond a fast pulse detector is needed capable of detecting both the Ti:Sa pulses and the light signals generated by the electron bunches. In the measurements done so far a photomultiplier with a rise time of 700 ps (Hamamatsu model H6780) has been used to detect the Ti:Sa pulses and the optical transition radiation pulses of the bunches. The narrow time range was then scanned in 0.5 ps steps.

2 Electro-Optic Effects in Anisotropic Crystals

For a homogeneous medium the electric displacement vector is given by

$$\mathbf{D} = \varepsilon_0 \varepsilon \mathbf{E} \tag{1}$$

where the (relative) dielectric permittivity ε is a scalar quantity (independent of direction). In a crystal the polarization may depend on the direction of the electric field with respect to the crystallographic axes. In this case the permittivity is a symmetric tensor $\widehat{\boldsymbol{\varepsilon}}$ and $\mathbf{D}$ is in general not parallel to the electric field. It is always possible to carry out a principal-axis transformation to an orthogonal coordinate system in which $\mathbf{E}$ and $\mathbf{D}$ are related by a diagonal matrix

$$\begin{pmatrix} D_1 \\ D_2 \\ D_3 \end{pmatrix} = \varepsilon_0 \begin{pmatrix} \varepsilon_1 & 0 & 0 \\ 0 & \varepsilon_2 & 0 \\ 0 & 0 & \varepsilon_3 \end{pmatrix} \cdot \begin{pmatrix} E_1 \\ E_2 \\ E_3 \end{pmatrix} . \tag{2}$$

If the ε_i are not all identical the crystal exhibits birefringence (double refraction).
The energy density of the electric field is $w_e = \frac{1}{2}\mathbf{E} \cdot \mathbf{D}$. Using eq. (2) we can show that the surfaces of constant energy density are ellipsoids in the $\mathbf{D}$ space:

$$\varepsilon_0 \, w_e = \mathbf{D} \cdot \widehat{\boldsymbol{\varepsilon}}^{-1} \cdot \mathbf{D} = \frac{D_1^2}{\varepsilon_1} + \frac{D_2^2}{\varepsilon_2} + \frac{D_3^2}{\varepsilon_3} \, . \tag{3}$$

Defining a dimensionless vector along the direction of $\mathbf{D}$ by $\mathbf{u} = \mathbf{D}/\sqrt{2\varepsilon_0 w_e}$ we get the equation of the refractive index ellipsoid

$$\frac{u_1^2}{n_1^2} + \frac{u_2^2}{n_2^2} + \frac{u_3^2}{n_3^2} = 1 \tag{4}$$

where as usual $n_i = \sqrt{\varepsilon_i}$ for a nonmagnetic material. Defining the impermeability tensor by

$$\widehat{\boldsymbol{\eta}} = \widehat{\boldsymbol{\varepsilon}}^{-1} \tag{5}$$

the ellipsoid equation can be written as

$$\mathbf{u}\cdot\widehat{\boldsymbol{\eta}}\cdot\mathbf{u} = 1 \; . \tag{6}$$

2.1 Electro-optic effect in zinc telluride

Zinc telluride has a cubic crystal lattice and is optically isotropic at vanishing electric field which means that the impermeability tensor can be replaced by the scalar quantity ε^{-1}, multiplied with the unit matrix $\mathbf{I}$. In the presence of an electric field the permeability tensor becomes

$$\widehat{\boldsymbol{\eta}}(\mathbf{E}) = \varepsilon^{-1}\,\mathbf{I} + \mathbf{r}\cdot\mathbf{E} \; . \tag{7}$$

The second term describes the Pockels effect. The Kerr effect which is quadratic in the electric field is neglected here. The ellipsoid equation is hence

$$\mathbf{u}\cdot\widehat{\boldsymbol{\eta}}(\mathbf{E})\cdot\mathbf{u} = \sum_{i,j=1,2,3}\left(\varepsilon^{-1}\delta_{ij} + \sum_{k=1,2,3} r_{ijk}E_k\right)u_i u_j = 1 \; . \tag{8}$$

The tensor $\widehat{\boldsymbol{\eta}}$ is symmetric, hence $r_{ijk} = r_{jik}$. It is convention to replace the first two indices i, j of the tensor $\mathbf{r}$ by a single index:

$(1,1) \to 1$	$r_{11k} \to r_{1k}$
$(2,2) \to 2$	$r_{22k} \to r_{2k}$
$(3,3) \to 3$	$r_{33k} \to r_{3k}$
$(2,3) \to 4$	$r_{23k} = r_{32k} \to r_{4k}$
$(1,3) \to 5$	$r_{13k} = r_{31k} \to r_{5k}$
$(1,2) \to 6$	$r_{12k} = r_{21k} \to r_{6k}$

ZnTe crystallizes in the zincblende structure (two face-centered cubic lattices which are shifted against each other by one quarter of the spatial diagonal). Owing to the high degree of symmetry, the ZnTe crystal is optically isotropic at vanishing electric fields, i.e. $n_1 = n_2 = n_3 = n_0$. In addition, the tensor $\mathbf{r}$ contains only one independent element: $r_{41} = r_{52} = r_{63}$. Hence the equation of the refractive index ellipsoid assumes the form

$$\frac{1}{n_0^2}(u_1^2 + u_2^2 + u_3^2) + 2r_{41}(E_1u_2u_3 + E_2u_3u_1 + E_3u_1u_2) = 1 \; . \tag{9}$$

To obtain the modified refractive indices one has to perform a principal-axis transformation.

2.2 Determination of the main refractive indices

The ZnTe crystals used in EOS experiments are cut in the (110) plane as shown in Fig. 1. The THz pulse and the laser pulse impinge perpendicular to this plane along the direction $[-1, -1, 0]$, their electric vectors lie therefore in the (110) plane. We define a

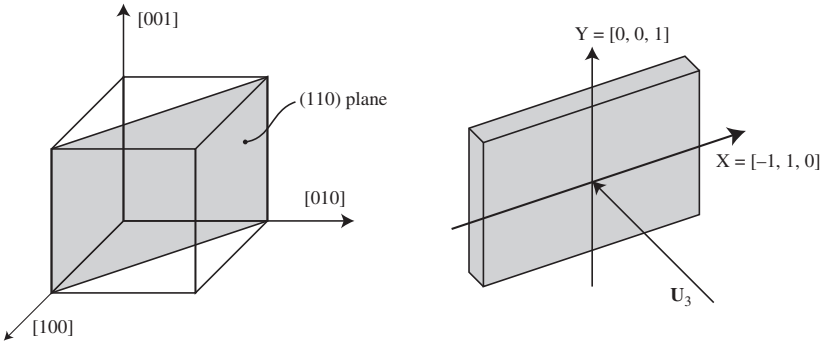

Figure 1: *Left: The (110) plane in the cubic zinc telluride crystal. Right: The coordinate system (X, Y) in the (110) plane. The THz and laser pulses impinge along the direction* $\mathbf{U_3}$ *which is the normal to this plane.*

two-dimensional coordinate system (X, Y) in this plane where X points along the [-1,1,0] direction and Y along the [0,0,1] direction.

Let the electric vector $\mathbf{E_a}$ of the THz pulse enclose an angle α with the X axis (the $[-1, 1, 0]$ axis of the ZnTe crystal). Its components in the base system of the cubic crystal lattice are

$$\mathbf{E_a} = E_a \begin{pmatrix} -\cos\alpha/\sqrt{2} \\ \cos\alpha/\sqrt{2} \\ \sin\alpha \end{pmatrix} . \tag{10}$$

Equation (9) reads in this special case

$$\mathbf{u}\cdot\widehat{\boldsymbol{\eta}}(\mathbf{E_a})\cdot\mathbf{u} = 1$$

with the field-dependent impermeability tensor

$$\widehat{\boldsymbol{\eta}}(\mathbf{E_a}) = \frac{1}{n_0^2}\begin{pmatrix} 1 & 0 & 0 \\ 0 & 1 & 0 \\ 0 & 0 & 1 \end{pmatrix} + r_{41}E_a \begin{pmatrix} 0 & \sin\alpha & \cos\alpha/\sqrt{2} \\ \sin\alpha & 0 & -\cos\alpha/\sqrt{2} \\ \cos\alpha/\sqrt{2} & -\cos\alpha/\sqrt{2} & 0 \end{pmatrix} . \tag{11}$$

The eigenvalues of the tensor are

$$\lambda_{1,2} = \frac{1}{n_0^2} - \frac{r_{41}E_a}{2}\left(\sin\alpha \pm \sqrt{1+3\cos^2\alpha}\right) , \quad \lambda_3 = \frac{1}{n_0^2} + r_{41}E_a\sin\alpha . \tag{12}$$

and the normalized eigenvectors

$$\begin{aligned} \mathbf{U_1} &= \frac{1}{2}\sqrt{1+\frac{\sin\alpha}{\sqrt{1+3\cos^2\alpha}}}\begin{pmatrix} -1 \\ 1 \\ \frac{2\sqrt{2}\cos\alpha}{\sqrt{1+3\cos^2\alpha}+\sin\alpha} \end{pmatrix} \\ \mathbf{U_2} &= \frac{1}{2}\sqrt{1-\frac{\sin\alpha}{\sqrt{1+3\cos^2\alpha}}}\begin{pmatrix} 1 \\ -1 \\ \frac{2\sqrt{2}\cos\alpha}{\sqrt{1+3\cos^2\alpha}-\sin\alpha} \end{pmatrix} \\ \mathbf{U_3} &= \frac{1}{\sqrt{2}}\begin{pmatrix} -1 \\ -1 \\ 0 \end{pmatrix} . \end{aligned} \tag{13}$$

The principal axes point in the direction of the eigenvectors. The main refractive indices are given by

$$n_i = 1/\sqrt{\lambda_i}\ .$$

Considering that $r_{41}E_a \ll 1/n_0^2$ this yields in good approximation

$$\begin{aligned} n_1 &= n_0 + \frac{n_0^3 r_{41} E_a}{4}\left(\sin\alpha + \sqrt{1+3\cos^2\alpha}\right) \\ n_2 &= n_0 + \frac{n_0^3 r_{41} E_a}{4}\left(\sin\alpha - \sqrt{1+3\cos^2\alpha}\right) \\ n_3 &= n_0 - \frac{n_0^3 r_{41} E_a}{2}\sin\alpha\ . \end{aligned} \tag{14}$$

From eq. (13) it is obvious that the third principal axis is perpendicular to the (110) crystal plane[1]. This is also the direction of incidence of the THz pulse and the Ti:Sa Laser pulse. The vector $\mathbf{U_1}$ lies in the (110) plane and encloses an angle ψ with the [-1,1,0] axis which can be calculated using the scalar product. Using the relation $\cos(2\psi) = 2\cos^2\psi - 1$ one gets

$$\cos 2\psi = \frac{\sin\alpha}{\sqrt{1+3\cos^2\alpha}}\ . \tag{15}$$

The second principal axis is parallel to the vector $\mathbf{U_2}$ and of course perpendicular to $\mathbf{U_1}$. Note that some care is needed to evaluate the vector $\mathbf{U_2}$ in the limit $\alpha \to \pi/2$ since the normalization factor vanishes here while the third component tends to infinity. One finds

$$\mathbf{U_2}\left(\frac{\pi}{2}\right) = \begin{pmatrix} 0 \\ 0 \\ 1 \end{pmatrix}\ .$$

So for $\alpha = \pi/2$ the principal axis $\mathbf{U_1}$ points in the X direction, and the axis $\mathbf{U_2}$ in the Y direction.

The principal refraction indices corresponding to the first two principal axes are n_1 and n_2. The refractive index ellipse is shown in Fig. 2.

The Ti:Sa laser beam is incident on the ZnTe crystal along the direction $[-1,-1,0]/\sqrt{2}$ (eigenvector $\mathbf{U_3}$). Its electric vector $\mathbf{E}_b$ lies therefore in the (110) plane. In the crystal of thickness d the two components of $\mathbf{E}_b$ along the principal axes $\mathbf{U_1}$ and $\mathbf{U_2}$ receive a relative phase shift

$$\Gamma(\alpha) = \frac{\omega\, d}{c}(n_1 - n_2) = \frac{\omega\, d}{2c}\, n_0^3\, r_{41} E_a \sqrt{1+3\cos^2\alpha} \tag{16}$$

where ω is the angular frequency of the laser light. The rotation angle ψ of the index ellipse in the (X,Y) plane, the main refractive indices and the relative phase shift are plotted in Fig. 3 as a function of the angle α between the electric vector $\mathbf{E}_a$ of the THz field and the X axis. The larger index corresponds to a slower speed of the light, the smaller index to a faster speed. Hence it is customary to designate the refractive indices also by $n_s = n_1$, $n_f = n_2$.

[1]The normal to this plane is the unit vector $\mathbf{U_3}$.

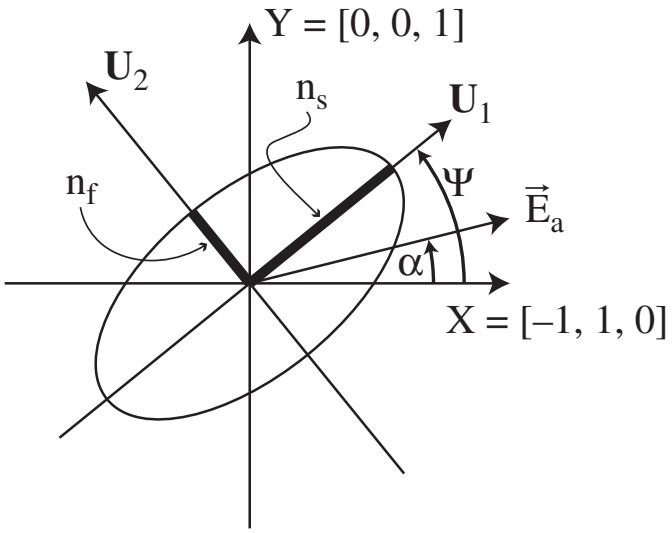

Figure 2: *The refractive index ellipsoid projected onto the (110) plane of the zinc telluride crystal. The difference between the refractive indices n_s and n_f is strongly exaggerated. The electric vector* $\mathbf{E_a}$ *encloses an angle α with the $X = [-1, 1, 0]$ axis of the ZnTe crystal while the angle between the long half axis of the ellipse and the X axis is given by $\psi(\alpha)$. Both the THz and laser pulses impinge along the normal to the (110) plane, given by the unit vector* $\mathbf{U_3} = (-1/\sqrt{2}, -1/\sqrt{2}, 0)$.

2.3 Principle of signal detection

2.3.1 Jones matrices

Usually the crystals have the shape of a square or rectangle with one edge parallel to the $X \simeq [-1, 1, 0]$ direction, the other one parallel to the $Y \simeq [0, 0, 1]$ axis. The Ti:Sa laser beam with electric vector $\mathbf{E}_b$ impinges along the normal of this plane which coincides with the principal axis $\mathbf{U}_3$. The propagation of a polarized light beam through a train of polarizers and birefringent plates is conveniently described using the Jones calculus, see e.g. [4]. Laser light with horizontal resp. vertical linear polarization is represented by the vectors

$$\mathbf{E_h} = E_b \begin{pmatrix} 1 \\ 0 \end{pmatrix} , \quad \mathbf{E_v} = E_b \begin{pmatrix} 0 \\ 1 \end{pmatrix} . \tag{17}$$

A rotation of the polarization plane by an angle φ is accomplished by the matrix

$$\mathbf{R}(\varphi) = \begin{pmatrix} \cos\varphi & \sin\varphi \\ -\sin\varphi & \cos\varphi \end{pmatrix} . \tag{18}$$

The matrix of the birefringent ZnTe crystal with the indices $n_s = n_1(\alpha)$, $n_f = n_2(\alpha)$ and thickness d reads in the principal-axis coordinate system

$$\mathbf{ZT} = \begin{pmatrix} \exp(-i\, n_s\, \omega\, d/c) & 0 \\ 0 & \exp(-i\, n_f\, \omega\, d/c) \end{pmatrix} .$$

If we separate out the average phase change $\phi = (n_s + n_f)\omega\, d/(2c)$ we get

$$\mathbf{ZT} = \mathbf{ZT}(\alpha) = \exp(-i\,\phi) \begin{pmatrix} \exp(-i\Gamma(\alpha)/2) & 0 \\ 0 & \exp(+i\Gamma(\alpha)/2) \end{pmatrix} \tag{19}$$

where $\Gamma = \Gamma(\alpha)$ is given by eq. (16). The phase factor $\exp(-i\phi)$ drops out when one calculates intensities and is therefore omitted in the following. With the help of the 2×2 unit matrix $\mathbf{I}$ and the matrix

$$\mathbf{J} = \begin{pmatrix} -i & 0 \\ 0 & i \end{pmatrix}$$

which has the nice property that $\mathbf{J^2} = -\mathbf{I}$, the ZnTe matrix can be written in the convenient form

$$\mathbf{ZT}(\alpha) = \mathbf{I} \cdot \cos\left(\frac{\Gamma(\alpha)}{2}\right) + \mathbf{J} \cdot \sin\left(\frac{\Gamma(\alpha)}{2}\right) \ . \tag{20}$$

The matrix of a quarter wave plate is

$$\mathbf{Q} = \begin{pmatrix} \exp(-i\pi/4) & 0 \\ 0 & \exp(+i\pi/4) \end{pmatrix} \ . \tag{21}$$

2.3.2 Detection schemes

We discuss two frequently employed detection schemes: crossed polarizers and balanced diode detectors. For simplicity the incident laser beam is assumed to be horizontally polarized, so it is represented by the vector

$$\mathbf{E_b} = E_b \begin{pmatrix} 1 \\ 0 \end{pmatrix} \ .$$

The effect of the ZnTe crystal is calculated as

$$E_b \cdot \mathbf{R}(-\psi) \cdot \mathbf{ZT} \cdot \mathbf{R}(\psi) \cdot \begin{pmatrix} 1 \\ 0 \end{pmatrix} \ . \tag{22}$$

This equation means that first the electric vector of the laser light is rotated into the coordinate sytem of the index ellipsoid, then the phase retardation is applied and finally the electric vector is rotated back to the (X, Y) system. The angle $\psi = \psi(\alpha)$ is given by eq. (15).

When we use a crossed (i.e. vertical) polarizer we multiply this expression from the left by the vector (0 1). The electric field measured behind this polarizer is given by

$$E_b \cdot \begin{pmatrix} 0 & 1 \end{pmatrix} \cdot \mathbf{R}(-\psi(\alpha)) \cdot \mathbf{ZT}(\alpha) \cdot \mathbf{R}(\psi(\alpha)) \cdot \begin{pmatrix} 1 \\ 0 \end{pmatrix} \ .$$

Inserting eq. (20) we find that the intensity S measured in a detector (diode or photomultiplier) is given by

$$S(\alpha) = E_b^2 \cdot \sin^2(2\,\psi(\alpha)) \, \sin^2\left(\frac{\Gamma(\alpha)}{2}\right) \ . \tag{23}$$

We will immediately see that a better sensitivity can be achieved with a balanced diode detector. For that purpose the light behind the ZnTe crystal is passed through a quarter wave plate whose main axes are oriented at $\pm 45°$ with respect to the horizontal direction. This means we have to multiply eq. (22) from the left with

$$\mathbf{R}(-\pi/4) \cdot \mathbf{Q} \cdot \mathbf{R}(\pi/4) \ .$$

A Wollaston prism, rotated by 45°, separates the two polarization components and guides them to the two diodes of a balanced detector. The arrangement is sketched in Fig. 4.

If the Terahertz field is absent the Ti:Sa laser pulse remains unaffected by the ZnTe crystal and leaves it with horizontal polarization. The quarter wave plate transforms this to circular polarization. The Wollaston prism guides the two orthogonal components of the circular wave to the two diodes which record then of course the same intensity. Hence the difference signal vanishes. With a finite Terahertz field, however, the radiation behind the ZnTe crystal is elliptically polarized leading to an imbalance between the two diode signals. For the special case $\alpha = 0$ we get $\psi = \pi/4$. Then the following expressions are easily evaluated:

$$\hat{I} = \mathbf{R}(-\frac{\pi}{4})\cdot\mathbf{Q}\cdot\mathbf{R}(\frac{\pi}{4})\cdot\mathbf{R}(-\psi)\cdot\mathbf{I}\cdot\mathbf{R}(\psi) = \frac{1}{\sqrt{2}}\begin{pmatrix} 1 & -i \\ -i & 1 \end{pmatrix} ,$$

$$\hat{J} = \mathbf{R}(-\frac{\pi}{4})\cdot\mathbf{Q}\cdot\mathbf{R}(\frac{\pi}{4})\cdot\mathbf{R}(-\psi)\cdot\mathbf{J}\cdot\mathbf{R}(\psi) = -\frac{1}{\sqrt{2}}\begin{pmatrix} 1 & i \\ i & 1 \end{pmatrix} .$$

The laser amplitude seen in diode 1 resp. diode 2 is

$$\begin{aligned} A_1 &= E_b \begin{pmatrix} 1 & 0 \end{pmatrix} \cdot \Big(\hat{I}\cos(\Gamma/2) + \hat{J}\sin(\Gamma/2)\Big) \cdot \begin{pmatrix} 1 \\ 0 \end{pmatrix} = E_b \frac{1}{\sqrt{2}} \left(\cos(\Gamma/2) - \sin(\Gamma/2)\right) \\ A_2 &= E_b \begin{pmatrix} 0 & 1 \end{pmatrix} \cdot \Big(\hat{I}\cos(\Gamma/2) + \hat{J}\sin(\Gamma/2)\Big) \cdot \begin{pmatrix} 1 \\ 0 \end{pmatrix} = -E_b \frac{i}{\sqrt{2}} \left(\cos(\Gamma/2) + \sin(\Gamma/2)\right) . \end{aligned}$$

The difference signal is

$$|A_1|^2 - |A_2|^2 = E_b^2 \sin(\Gamma) .$$

For $\alpha \neq 0$ the computation is a bit more complicated but the conclusion remains valid that the difference signal in the balanced diode detector is

$$|A_1(\alpha)|^2 - |A_2(\alpha)|^2 \propto \sin(\Gamma(\alpha)) . \tag{24}$$

In conventional Terahertz spectroscopy the field E_a is usually so weak that $\Gamma \ll 1$. Then the signal obtained with the balanced detector is much larger than the signal observed in the crossed polarizer geometry. In Fig. 5 we plot the expected signals for a reasonable set of parameters as a function of the angle α between the electric vector of the Terahertz field and the [-1,1,0] axis of the ZnTe crystal. The optimum orientation is $\alpha = 0$.

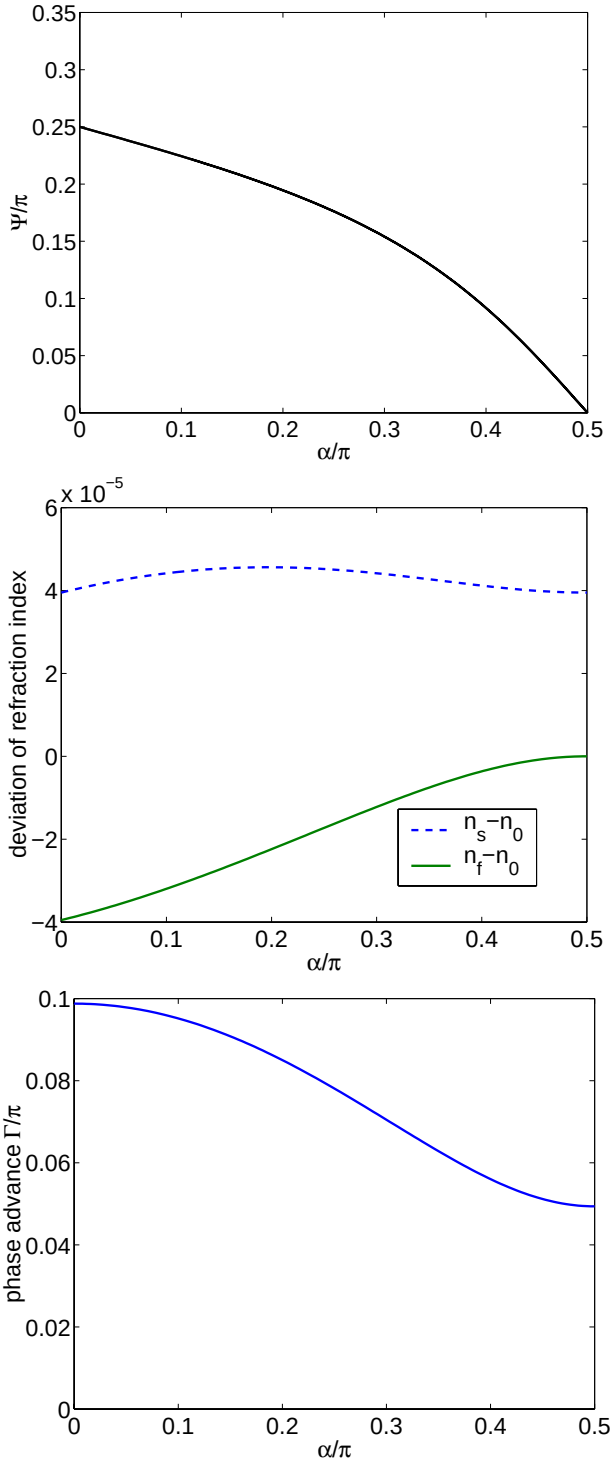

Figure 3: *Top: The angle ψ between the first principal axis of the refractive index ellipsoid and the X axis as a function of the angle α between the electric vector $\mathbf{E}_a$ of the THz field and the X axis. Middle: The refractive indices $(n_s(\alpha) - n_0)$ and $(n_f(\alpha) - n_0)$, plotted versus α. Bottom: The relative phase shift $\Gamma(\alpha)$ between the two orthogonal components of the laser field $\mathbf{E}_b$. The curves are computed for a ZnTe crystal of $d = 0.5$ mm thickness and a THz field $E_a = 0.9 \cdot 10^6$ V/m.*

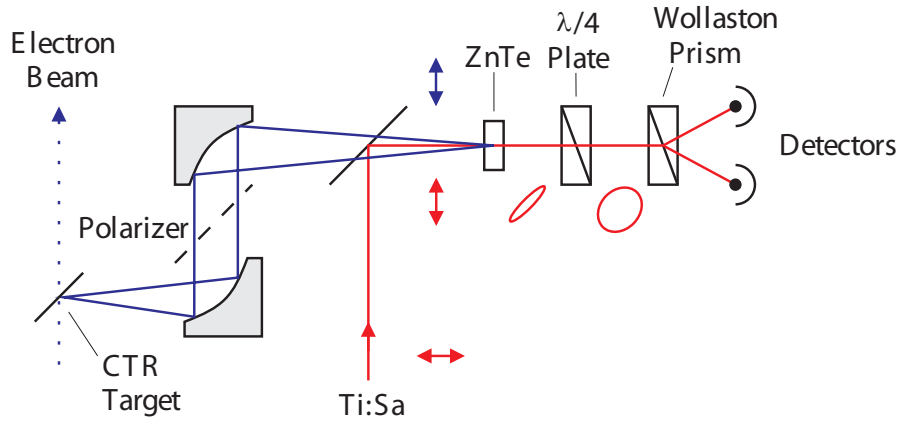

Figure 4: *Simplified view of electro-optic signal detection using a quarter wave plate, a Wollaston prism and a balanced diode detector. The laser is polarized horizontally. The quarter wave plate, the Wollaston prism and the balanced detector are rotated by* 45° *with respect to the horizontal plane.*

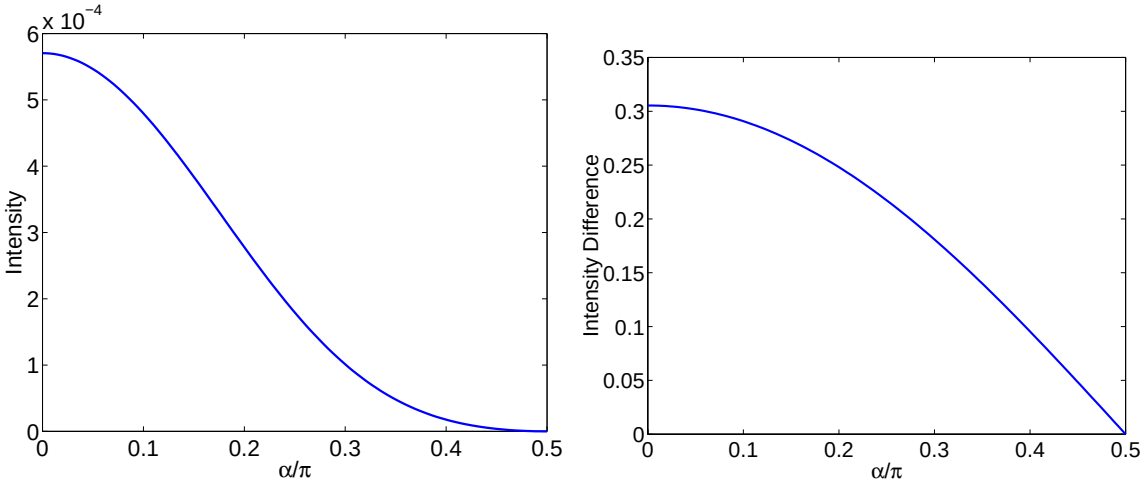

Figure 5: *The EOS signals for the crossed-polarizer arrangement (left) and for the balanced diode detector arrangement (right) as a function of the angle* α *between the electric vector of the Terahertz field and the* $X = [-1, 1, 0]$ *axis of the ZnTe crystal.*

3 Experimental Setup

3.1 General description of the EOS setup at TTF

An overview of the electro-optic bunch diagnostic system at the TESLA test accelerator is shown in Fig. 6. The electron linac is installed in the DESY hall 3. The Ti:Sa laser

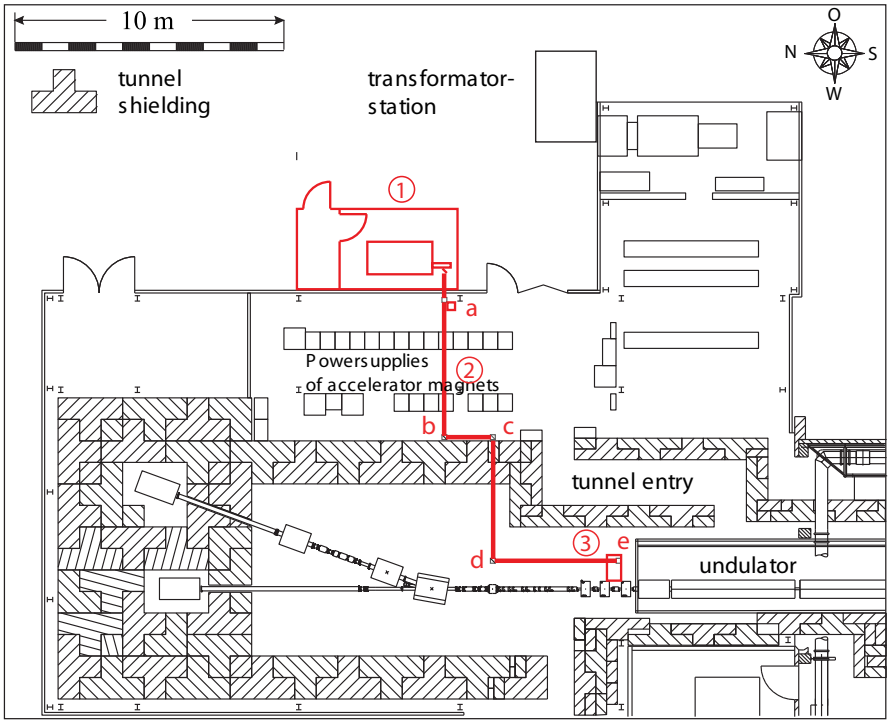

Figure 6: *The experimental setup and the laser beam line at the TTF linac. (1) Laser container, (2) optical transfer channel, (3) optical table in the accelerator tunnel.*

system together with the optical components is mounted on an optical table in a container outside hall 3. The container is temperature stabilized by an air conditioner to 23 ± 1 °C and is equipped with an outer reflective cover which prevents heating by sun radiation. A 20 m long optical transfer channel equipped with 8 silver coated mirrors transports the laser beam into the accelerator area. A second optical table is installed close to the electron beam. The ZnTe crystal and the detectors are mounted on this table. Coherent transition radiation is extracted through a polycrystalline quartz window and focused onto the ZnTe crystal. A schematic view of the overall optical system is given in Fig. 7. The components are described in detail in the next sections.

3.2 Ti:Sa laser system

The main component of the experimental setup is a mode-locked titanium-sapphire laser with a specified pulse duration of 15 fs (Femtosource Compact 20, made by Femtolasers, Vienna). The wavelength range is (805 ± 35) nm. The Ti:Sa laser is pumped by a 5 W diode-pumped frequency-doubled Nd:YVO_4 laser (Verdi 5 W, made by COHERENT). The pump laser runs in the continuous wave (cw) mode and emits green light at $\lambda =$

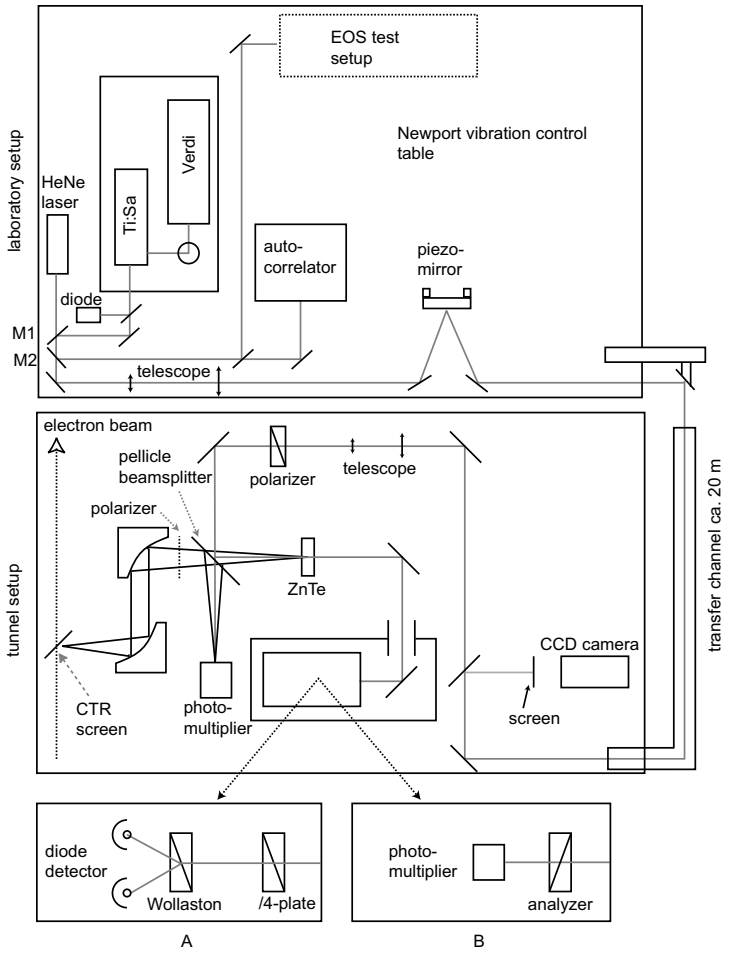

Figure 7: *The optical setups in the laser container and in the accelerator tunnel.*

532 nm. The technical specifications of the lasers are summarized in Appendix A. The Nd:YVO_4 head of the Verdi laser is mounted on a water cooled chiller plate keeping the temperature at $23 \pm 0.5°C$. The Ti:Sa laser is mounted in a common box with the pump laser and is temperature stabilized by the cooling system of the pump laser. Optical input into the Ti:Sa laser is made by two adjustable mirrors and a periscope for height adjustment and polarization rotation. Both lasers are mounted on an optical table in a temperature stabilized container.

3.2.1 Principle of Ti:Sa laser

The generation of ultrashort laser pulses requires a laser medium whose gain curve extends over a sufficiently large wavelength range. A suitable material is titanium-doped sapphire (Al_2O_3) in which a small percentage of the Al^{3+} ions are replaced by Ti^{3+} ions. The Ti:Sa crystal has a broad fluorescence band centered at 800 nm and a wide absorption band around 500 nm which yields a good pumping efficiency with green laser light (Fig. 8). The crystal features good mechanical strength and high heat conductivity which makes it suitable for high power lasing. In the Femtosource Compact 20, the laser gain exceeds the

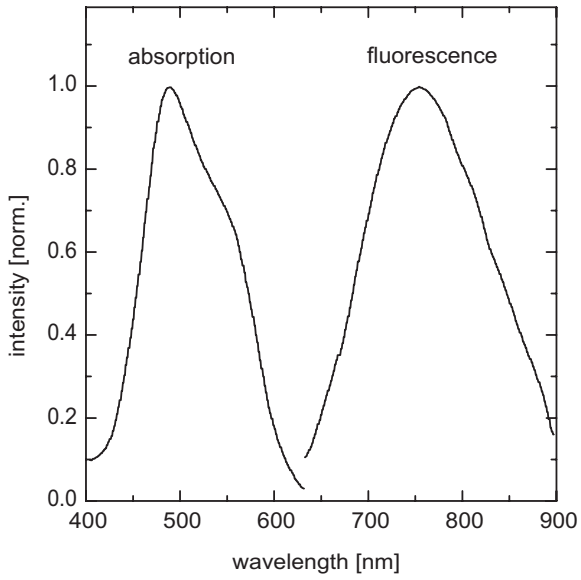

Figure 8: *Absorption and fluorescence of titanium-sapphire as a function of wavelength.*

.

resonator losses in the wavelength range 770 to 840 nm. Usually all longitudinal resonator modes in this range are excited by the pump laser but with random phase relations among them. Hence the Ti:Sa laser runs in the cw mode without a pulse structure. In order to achieve short pulses the phases of the various modes must be rigidly coupled. Passive mode-locking is achieved by modulating the resonator losses with the difference frequency of neighbouring modes. In that case each mode excites its side bands which coincide with the two adjacent modes and enforce a phase-locked oscillation onto these modes. Since this happens for all modes within the gain region one obtains eventually a fixed phase relation between all of them.

Call L the length of the round trip in the optical resonator. Then $f_{rev} = c/L$ is the revolution frequency of the photons in the resonator which is identical with the laser repetition frequency in pulsed-mode operation. The longitudinal optical modes have eigenfrequencies f_n which are very high harmonics of the revolution frequency. For the Femtosource Compact laser with $f_{rev} = 81$ MHz

$$f_n = n \cdot f_{rev} \quad \text{with} \quad 4.4 \cdot 10^6 < n < 4.8 \cdot 10^6 \,. \tag{25}$$

3.2.2 Loss modulation by the Kerr effect

The difference frequency of neighbouring modes is just the revolution frequency. A loss modulation at this frequency can be achieved by making use of the Kerr effect. Titanium doped sapphire is an electro-optical crystal, the refractive index varies with the square of the electric field of the light wave

$$n(E) = n_0 + n_2 E^2 \,. \tag{26}$$

In transverse direction the laser beam has a gaussian profile, so the intensity is higher at the center of the beam than at the rim. At sufficiently high laser power the Ti:Sa crystal

acquires a higher index of refraction on the beam axis and acts as a focusing lens (the so-called Kerr lens), see Fig.9 for an illustration. Suppose now that in a cw laser beam a local intensity enhancement is created. This peak travels in the resonator with the revolution frequency and is focused by the Kerr lens due to its higher electric field. If now an aperture is introduced which produces losses for the unfocused part of the beam but leaves the focused beam unaffected one gets the required loss modulation at the difference frequency of neighbouring modes.

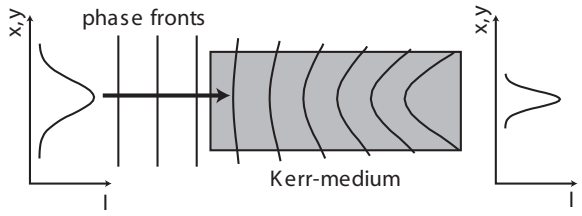

Figure 9: *Illustration of the Kerr lens effect.*

.

Strong intensity enhancements do not occur spontaneously but are usually induced from the outside. A common method is to make a sudden movement of the end mirror of the optical resonator which leads to intensity fluctuations.

3.2.3 Phase modulation and pulse compression to the fs level

The Kerr effect in the Ti:Sa crystal results in different phase velocities of the various optical eigenmodes. A wave packet therefore spreads in time, it acquires a positive chirp (the long wavelengths are at the front, the short ones at the rear end). A pulse compression can be done with prisms. For ultrashort pulses special multilayer mirrors, so-called chirped mirrors are used which reflect short wavelengths at the front layer and longer wavelengths at deeper layers (Fig. 10). The Femtosource Compact achieves a pulse length of 15 fs corresponding to the lower limit given by the Fourier theorem.

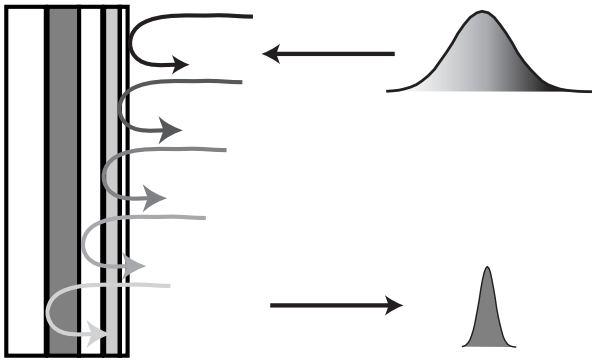

Figure 10: *Laser pulse compression using a chirped mirror.*

.

3.2.4 Layout of Femtolaser

The layout of the Femtosource Compact laser is shown in Fig. 11. The Ti:Sa crystal is arranged between two focusing mirrors to achieve the power density needed for the Kerr lens effect. The pulsed beam is better focused in the crystal than the cw beam, hence it has a better overlap with the pump radiation. This leads automatically to the loss modulation at the difference frequency of adjacent modes. The end mirror of the resonator is movable: a piezo-electric actuator permits fast variation of the revolution frequency by 12 kHz. This is utilized for the synchronization of the Ti:Sa repetition frequency to the accelerator RF by means of a phase-lock feedback loop. Larger frequency shifts can be realized with the help of a picomotor.

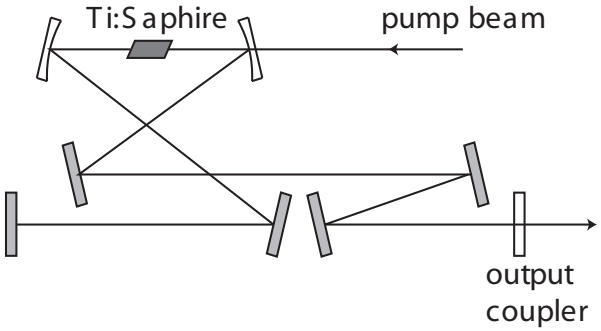

Figure 11: *Optical layout of the Femtosource Compact laser.*

.

3.3 Optical setup in the laser container

The optical table (Newport Vibration Control) rests on four concrete pillars and is vibration damped by air cushions. Figure 12 shows seismometric measurements of the table with and without air suspension. The box containing the Ti:Sa laser and the head of the Verdi pump laser is fixed on the table. In addition a helium-neon laser is installed for alignment purposes. The two lasers can be selected alternatively by means of a flippable mirror (mirror M1 in Fig. 7). The Ti:Sa beam crosses a beam splitter which reflects part of the intensity onto a fast InGaAs photodiode which is used to control proper mode-locking and to enable synchronization with the accelerator rf (radio frequency). The transmitted Ti:Sa beam is guided into a beam line which contains a variable attenuator, a two-lens telescope which widens the beam diameter (1 mm) by a factor of 6 and a piezo-controlled mirror for beam position stabilization. By a second flippable mirror (M2) the laser can be directed into an autocorrelator for pulse length measurement, or a test setup for the electro-optic detection system.

3.4 Transfer and stabilization of laser beam

The first element of the laser beam transfer is the beam widening telescope. In the accelerator area the beam is narrowed down to its original size by a corresponding telescope.

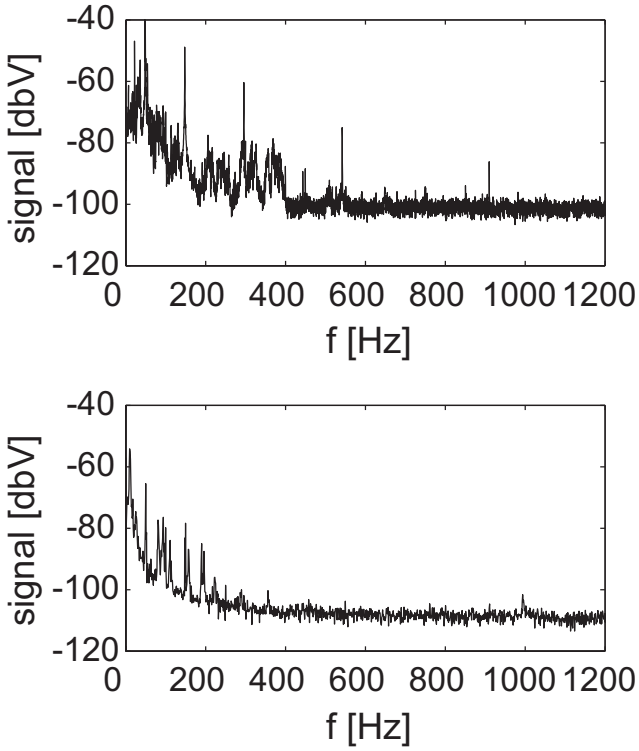

Figure 12: *Seismometric measurements on the optical table in the laser hut. Top: without air suspension. Bottom: with air suspension.*

The purpose of the telescopes is to reduce the sensitivity to height variations of the optical table and to mechanical vibrations of the mirrors in the transfer line. The transfer channel is about 20 m long and contains 8 adjustable mirrors of 50 mm diameter which are coated with silver and a protective dielectric layer. The reflectivity at 800 nm is better than 98%. According to the manufacturer (LINOS Photonics) the mirrors cause a negligible lenghtening of 15 fs pulses. The laser beam is transported in aluminium tubes. Two mirrors are needed to change the height of the beam above ground. These mirrors were first fixed at a vertical steel I-beam of the building. Since the vibrations caused by a near-by transformer station were unacceptable a sand-filled vertical pillar with rubber suspension (eigenfrequency < 7 Hz) was installed to hold these mirrors. The improvement can be seen in Fig. 13. The other mirrors of the transfer line are attached to the concrete shielding of the accelerator. The slow drift of the height of the optical table translates into beam offsets of up to 10 mm in the accelerator area. The piezo-controlled mirror is used to compensate these position variations. This can be done manually or by computer-control. A Mylar foil beam splitter on the optical table in the accelerator area reflects part of the widened laser beam onto a transparent screen. The image is recorded by a CCD camera and digitized by a frame grabber. A Matlab routine controls the adjustment of the piezo-mirror in a feedback loop. The measured time variation of the beam spot position with and without feedback control is shown in Fig.14. The beam transmitted by the Mylar foil is demagnified by the second telescope. The positional accuracy of the narrow beam is better than 0.1 mm.

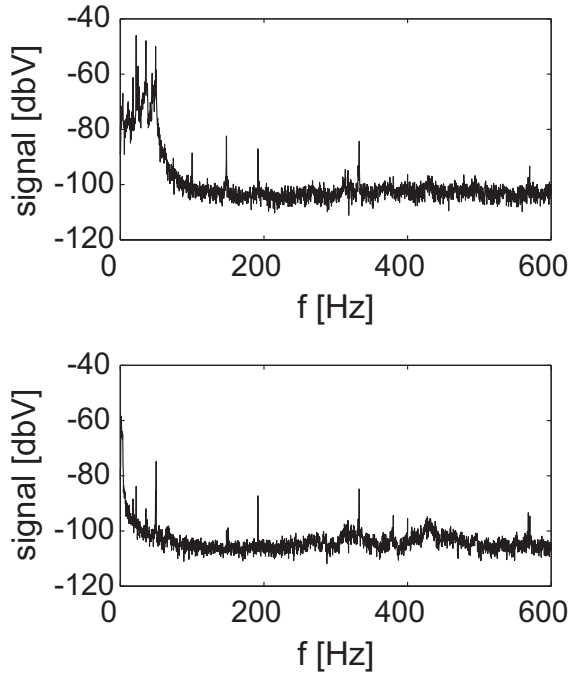

Figure 13: *Vibrational noise in laser beam transport. Top: at a mirror mounted to a vertical I-beam in Hall 3. Bottom: vibrational noise at a mirror mounted on a vibration-damped vertical pillar.*

.

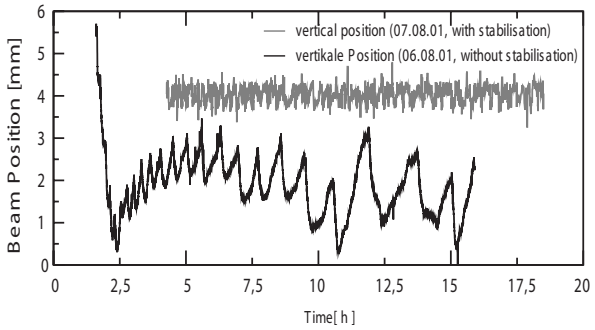

Figure 14: *Time variation of vertical laser beam position without and with feedback control.*

.

3.5 Optical setup in the accelerator area

The demagnifying telescope mentioned above is followed by a polarization filter which restores full horizontal polarization[2]. A foil beam splitter (pellicle beam splitter, made by Melles Griot) reflects half of the intensity of the demagnified laser beam onto the ZnTe crystal. The other half goes to the timing photomultiplier. The 100-1000 GHz transition radiation pulses of the electron bunches are imaged by two parabolic mirrors onto the

[2]The Femtosource laser has 100% horizontal linear polarization but some elliptic polarization is introduced by the optical components in the transfer line.

ZnTe crystal. A wire grid behind the second mirror transmits only the horizontal polarization component. The optical transition radiation pulse is focused by the same mirrors and, by means of the pellicle beam splitter, is directed onto the cathode of the timing photomultiplier. Of course part of the optical radiation penetrates also the ZnTe crystal and enters the detection system. The detector for the electro-optic signal is hermetically enclosed in an aluminium box of 10 mm wall thickness to protect it against the strong electromagnetic background which is caused by the wake fields of the electron bunches and reflected out of the beam vacuum pipe by the transition radiation foil. Without this Faraday cage the detectors showed strong, bunch-correlated signals which, however, were totally independent of the presence of the Ti:Sa laser beam. Having passed the ZnTe crystal the Ti:Sa laser beam is guided into the box through a 100 mm long aluminium tube of 8 mm diameter which acts as a high pass filter and removes all electromagnetics waves below 30 GHz.

3.6 Synchronization between TiSa laser and electron bunches

The synchronization system of the Ti:Sa laser (see Fig. 15) is based on a phase locked loop (PLL). The 81 MHz repetition frequency of the laser pulses is measured with a InGaAs-PIN-Diode with a bandwidth of 3.5 GHz. The diode converts the 15 femtosecond light pulses into electrical pulses with an amplitude of several hundred millivolts and a duration of several hundred picoseconds when terminated into 50 Ω. These short pulses contain harmonics up to very high order which allows to extract the 1.3 GHz Fourier component (16th harmonic of 81 MHz)) with a bandpass filter. The phase of the resulting 1.3 GHz component can be measured relative to the 1.3 GHz reference frequency of the accelerator to which the electron bunch generation and all rf systems of the linac are synchronized. This is accomplished with a double balanced mixer with a resolution of better than 0.1° at 1.3 GHz corresponding to a time resolution of better than 200 fs.

The repetition frequency of the laser pulses can be controlled with a movable mirror of the laser oscillator. The mirror position is controlled by a piezo-electric actuator and a picomotor. The frequency of the laser pulses is inversely proportional to the laser resonator length and can be varied by 750 Hz (corresponding to 12 KHz at 1.3 GHz) with the piezo actuator (0 - 100 V).

The phase locked loop is closed when the amplified and filtered phase error signal is connected to the input of the piezo actuator controller. Any timing error results in a change in laser frequency which then reduces the error. The steady state error is inversely proportional to the gain. An integrator in the filter for the error signal provides high gain at low frequencies and therefore a small steady state error.

The error is reduced by the (frequency) dependent gain of the controller by the factor

$$\frac{1}{1+G(s)} \quad \text{with} \quad G(s) = G_p + \frac{G_i}{s} \tag{27}$$

where G_p is the proportional gain and G_i the integrator gain.

At 300 Hz, where most of the microphonic noise occurred, the maximum gain achieved was approximately 10. The gain is limited by a mechanical resonance of the piezo actuator at 5 kHz. At maximum gain the residual timing fluctuation have been measured to be about 700 fs rms. In the meantime it has been found out that during the electro-optic

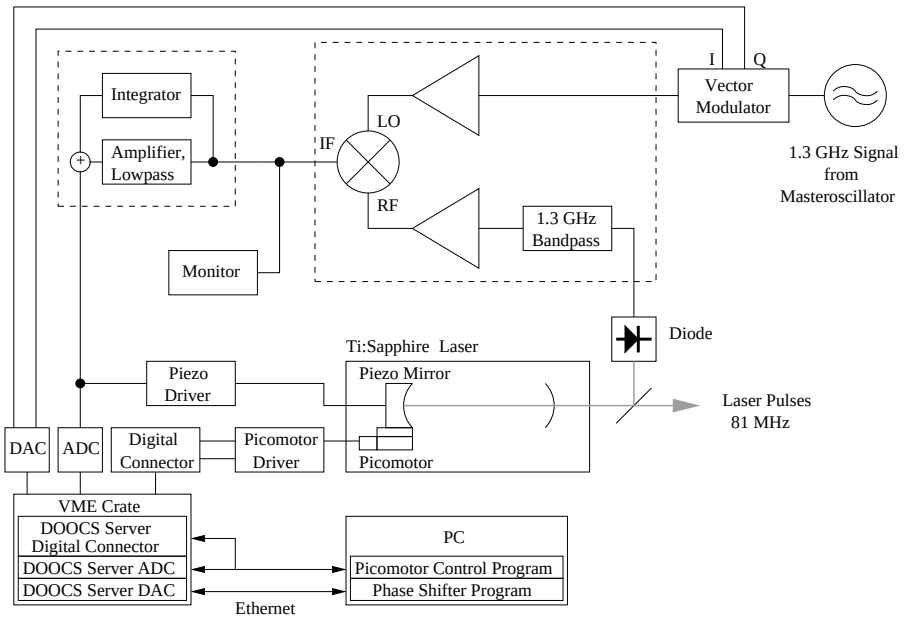

Figure 15: *Synchronization of Ti:Sa laser and bunched electron beam.*

.

measurements there was substantial noise on the rf signal from the master oscillator of the TTF radio frequency system. Reducing this noise and also the electromagnetic perturbations from ground loops it can be expected to obtain a time jitter of the synchronization loop of less than 200 fs.

4 Test Measurements with Electron Beam

The electro-optic detection is based on a measurement of the elliptic polarization of the optical probe pulse which is caused by the Pockels effect in the ZnTe crystal. Having passed the ZnTe crystal the laser beam traverses optical elements which transform the polarization information into an intensity information. The size of the EOS signal depends on the energy of the coherent transition radiation (CTR) pulse, the crystal orientation and the orientation of the polarization planes of the incoming CTR and Ti:Sa radiation.

4.1 Estimation of the CTR pulse energy

In the experiments at the TTF linac the electron energy was 240 MeV. As an example we consider an electron bunch which has a leading gaussian peak with $\sigma_t = 1$ ps and a charge of 0.25 nC ($N = 1.6 \cdot 10^9$ electrons). The transition radiation energy emitted into the backward hemisphere by a single electron crossing the OTR screen is independent of frequency

$$W_1 \equiv \frac{dW_1}{d\omega} = \frac{e^2}{2\pi^2 \varepsilon_0 c} \ln \gamma \,. \tag{28}$$

Here γ is the Lorentz factor. The charge distribution in the bunch

$$\rho(t) = \frac{N}{\sqrt{2\pi}\,\sigma} \exp\left(-\frac{t^2}{2\sigma_t^2}\right)$$

must be convoluted with the spectral distribution to obtain the coherent radiation emitted by a bunch of N electrons

$$\frac{dW_N}{d\omega} = W_1 \left| \int_{-\infty}^{+\infty} \rho(t)\, \exp(i\omega t)\, dt \right|^2 = N^2\, W_1\, \exp(-\sigma_t^2 \omega^2) \,. \tag{29}$$

The frequency range accepted by the experimental setup is about 80 to 800 GHz. Integration of (29) yields for the energy of the CTR pulse

$$W_{CTR} \approx 3\,\mu\mathrm{J} \,.$$

The CTR is focused by two parabolic mirrors with a focal length of $f = 200$ mm onto the ZnTe crystal. The radius of the THz beam at the second mirror is $R \approx 40$ mm. Assuming a gaussian beam and a wavelength $\lambda = 2$ mm the beam radius at the focus of the mirror is $r \approx 3$ mm. Then the instantaneous intensity of the $\Delta t = 2.3$ ps (FWHM) long CTR pulse in the focal region of the parabolic mirror is

$$I_{CTR} \approx \frac{W_{CTR}}{\pi r^2 \Delta t} \approx 4 \cdot 10^{10}\,\mathrm{W/m^2} \,.$$

A number of losses have to be considered. The transmission of the polarizing wire grid is about 50%. The absorption and transmission losses in the optical setup are estimated to be in the order of 50%. Moreover, half of the aperture has been blocked in the experiment to prevent a destructive interference of the radially polarized CTR radiation at the focal plane of the second mirror. Hence we assume an intensity of $I_{inc} = 5 \cdot 10^9\,\mathrm{W/m^2}$ that

is incident onto the ZnTe crystal. The dielectric constant of ZnTe is $\varepsilon_r = 10$ at THz frequencies. The transmitted intensity is

$$I_{trans} = \frac{4n}{(n+1)^2} I_{inc} \approx 4 \cdot 10^9 \,\mathrm{W/m^2}$$

where $n = \sqrt{\varepsilon_r}$. The electric field E_a in the ZnTe crystal is then

$$E_a = \sqrt{2 I_{trans}/(\varepsilon_0 \, n \, c)} \approx 0.9 \cdot 10^6 \ \mathrm{V/m} \ .$$

For such a terahertz field and a crystal thickness of 0.5 mm one obtains with $r_{41} = 4 \cdot 10^{-12}$m/V and a refractive index $n_0 = 2.8$ at 800 nm a maximum phase shift within the probe beam of

$$\Gamma \approx 0.1 \, \pi \mathrm{rad} \ . \tag{30}$$

4.2 Detector setup

To find the electro-optic signal several test measurements were performed with the two different detection schemes described in the previous section. In the first experiments a balanced diode detector was used but the signals suffered from large electromagnetic noise due to the wake fields generated by the bunched electron beam and reflected out of the vacuum chamber by the CTR target. For this reason the crossed polarizer arrangement was chosen with a photomultiplier as signal detector. The multiplier was enclosed in a hermetically shielded aluminum box to suppress the large electromagnetic background. The laser beam was guided into the box through a 100 mm aluminium long tube of 8 mm diameter which cut off all rf noise below 20 GHz. Using this setup data were taken in March and April 2002.

4.3 Procedure to find an overlap between laser and CTR pulse

One of the main difficulties of the electro-optic sampling experiment at the TTF-linac is the very low bunch repetition rate of 1 Hz. The measurements were done with only 1 or 2 bunches per macropulse.

To find the coincidence signal between the CTR signal of the bunch and a laser pulse it would in principle be necessary to scan the time interval of 12.3 ns between two successive laser pulses in steps of 1 ps. Since the data collection was made with a 20 Gs sampling oscilloscope with a readout time of about a second such a scan would have lasted several hours. To reduce the scan range substantially a " timing photomultiplier" with a rise time of 700 ps was utilized to determine the relative timing of the transition radiation signal and the laser pulses with an accuracy of better than 1000 ps. The setup is shown in Fig. 7. The optical setup ensures that both the laser pulses and the optical transition radiation (OTR) pulses have the same optical path length to the photocathode. To find the precise overlap with picosecond accuracy, a scan of the narrow time interval was carried out.

4.4 Experimental results

The data acquisition was done with a Tektronix TDS6604 digital oscilloscope with 20 GS/s data acquisition rate. The signal of the detector photomultiplier was transferred via GBIP

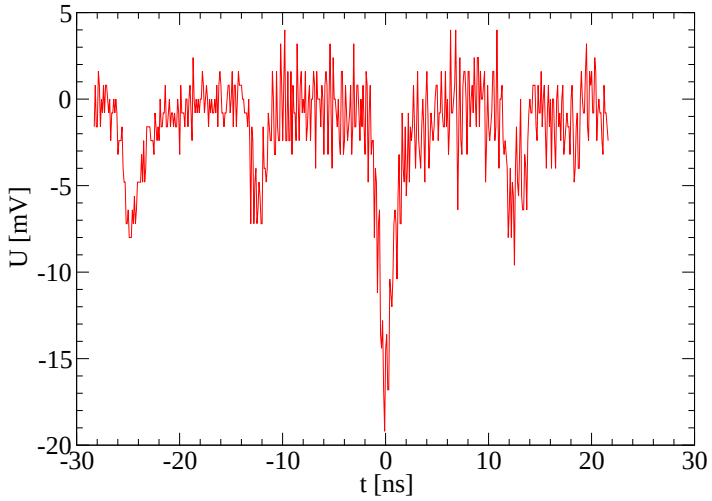

Figure 16: *Photomultiplier signal after establishing a coarse overlap between the Ti:Sa laser pulses and the optical transition radiation pulse (large signal at $t = 0$ ns).*

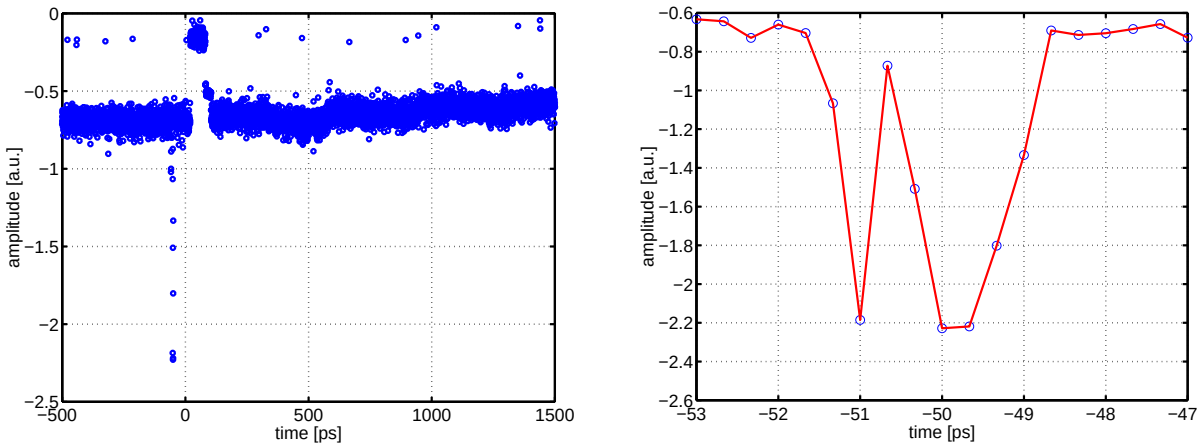

Figure 17: *Left: Scan of the overlap signal of the laser and OTR pulse over a time interval of 2000 ps. Right: Enlarged view of the overlap region of the Ti:Sa pulse and the CTR pulse.*

and Ethernet to a PC once per second and recorded by a LabView program. Figure 16 shows the signal after the coarse overlap (± 200 ps accuracy) of the laser and OTR pulse was established. The central peak with large amplitude is due to the overlapping laser and OTR pulses, whereas the small amplitude peaks are the non-overlapping laser pulses. The delay between the laser pulse and the OTR pulse was shifted in picosecond steps by means of a phase shifter in the rf synchronization system under the control of a Matlab program. In the first measurement an interval of $[-500\text{ ps}, 1500\text{ ps}]$ was scanned in 0.5 ps steps. In Fig. 17 the amplitude of the central peak of Fig. 16 is plotted versus the relative delay.

The points with amplitude values around 0.5 represent the coarsely overlapping laser and OTR pulses whereas the points with an amplitude near zero are caused by missing

OTR signals. In the latter case the electron beam failed briefly and therefore no OTR radiation hit the photomultiplier. The sharp peak at -50 ps is the searched electro-optic correlation signal between the laser pulse and the electron bunch. A zoomed view of this region is shown in the right-hand part of Fig. 17. The overlap has a length of roughly 3 ps. This result was reproduced in several measurements.

At present it is not yet possible to derive a bunch length from these data. The reason is that the measured time jitter in the synchronization loop between the Ti:Sa laser and the 1300 MHz radio frequency of the linac amounted to 700 fs rms. In the meantime it has been found out that part of this jitter was caused by a 100 Hz noise in the master oscillator of the TTF rf system. An improved master oscillator and a new synchronization electronics are under development.

The overlap curve shown in Fig. 17 is compatible with the longitudinal bunch shape known from interferometric measurements [5]. With the improved synchronization system and with an electro-optic setup where the ZnTe crystal is mounted inside the beam vacuum chamber a significantly improved time resolution can be expected.

The authors thank I. Wilke for her advice and help in the early stages of the EOS experiment. Thanks are also due to W.A. Gillespie, G. Knippels, A. MacLeod, V. Schlott and H. Sigg for stimulating discussions. The TU Darmstadt members of the collaboration are grateful for support within the framework of the Collaboration Agreement between DESY and TU Darmstadt. The financial support by the BMBF (Förderkennzeichen 05 HSOGU1/16) is gratefully acknowledged.

References

[1] Q. Wu, X.-C. Zhang, Appl. Phys. Lett. **67** (1995) 3523
Z. Jiang, X.-C. Zhang, Appl. Phys. Lett. **72** (1998) 1945 and IEEE J. Quant. Electr. **36** (2000) 1214

[2] X. Yan, A.M. MacLeod, W.A. Gillespie, G.H.M. Knippels, D. Oepts, A.F.G. van der Meer, W. Seidel, Phys. Rev. Lett. **85** (2000) 3404

[3] I. Wilke, A.M. MacLeod, W.A. Gillespie, G.H.M. Knippels, G. Berden, A.F.G. van der Meer, Phys. Rev. Lett. **88** (2002) 124801

[4] A. Yariv, *Optical Electronics in Modern Communications*, Oxford University Press 1977

[5] M. Hüning, DESY-Thesis-2002-029 (2002)

A Parameters of the Laser system

The parameters of the titanium-sapphire laser and the pump laser are summarized in the following table.

Pump laser	
manufacturer	Coherent
model	Verdi 5 W
type	diode pumped frequency doubled Nd:YVO_4 laser
operating mode	cw
output power	5 W
wavelength	532 nm (single mode)
spatial mode	TEM_{00}
beam diameter	2.25 mm
beam divergence	0.5 mrad
M^2	< 1.1
noise	$< 0.02\%$ rms
polarization	vertical, $> 100:1$
Ti:Sapphire laser	
manufacturer	Femtolasers, Vienna
model	Femtosource Compact 20
operating modes	cw, pulsed
pump power (typical)	3.5 W
output power (cw)	420 mW
output power (pulse)	> 300 mW
central wavelength	807 nm
bandwidth	65 nm
spatial mode	TEM_{00} ($M^2 < 1.3$)
beam diameter ($1/e^2$)	< 2 mm
beam divergence	< 2 mrad
pulse length	15 fs (FWHM)
repetition rate	81.25 MHz
rep. rate tuning	picomotor, piezo translator
polarization	horizontal, > 100:1